Free Radical Biology and Medicine 204 (2023) 215–225

Contents lists available at ScienceDirect

Free Radical Biology and Medicine

journal homepage: www.elsevier.com/locate/freeradbiomed

Structural and biochemical characterization establishes a detailed understanding of KEAP1-CUL3 complex assembly

Roslin J. Adamson [a,1], N Connor Payne [b,c,1], Sergio G. Bartual [a,2], Ralph Mazitschek [b,d,e,**], Alex N. Bullock [a,*]

[a] Centre for Medicines Discovery, Nuffield Department of Medicine, University of Oxford, Oxford, OX3 7FZ, UK
[b] Center for Systems Biology, Massachusetts General Hospital, Boston, MA, 02114, USA
[c] Department of Chemistry & Chemical Biology, Harvard University, Cambridge, MA, 02138, USA
[d] Harvard T.H. Chan School of Public Health, Boston, MA, 02115, USA
[e] Broad Institute of MIT and Harvard, Cambridge, MA, 02142, USA

ARTICLE INFO

Keywords:
KEAP1
BTB
Kelch
Cullin-RING ligase
Ubiquitin
TR-FRET

ABSTRACT

KEAP1 promotes the ubiquitin-dependent degradation of NRF2 by assembling into a CUL3-dependent ubiquitin ligase complex. Oxidative and electrophilic stress inhibit KEAP1 allowing NRF2 to accumulate for the trans-activation of stress response genes. To date there are no structures of the KEAP1-CUL3 interaction nor binding data to show the contributions of different domains to their binding affinity. We determined a crystal structure of the BTB and 3-box domains of human KEAP1 in complex with the CUL3 N-terminal domain that showed a heterotetrameric assembly with 2:2 stoichiometry. To support the structural data, we developed a versatile TR-FRET-based assay system to profile the binding of BTB-domain-containing proteins to CUL3 and determine the contribution of distinct protein features, revealing the importance of the CUL3 N-terminal extension for high affinity binding. We further provide direct evidence that the investigational drug CDDO does not disrupt the KEAP1-CUL3 interaction, even at high concentrations, but reduces the affinity of KEAP1-CUL3 binding. The TR-FRET-based assay system offers a generalizable platform for profiling this protein class and may form a suitable screening platform for ligands that disrupt these interactions by targeting the BTB or 3-box domains to block E3 ligase function.

1. Introduction

The Kelch-like family of E3 ubiquitin ligase adaptor proteins (KLHL1-42) comprising BTB, BACK and Kelch domains are associated with a wide range of chronic diseases, including autoimmune and inflammatory diseases, neurodegeneration and cancer [1–3]. Most studied as a therapeutic target is the protein KEAP1 (KLHL19), which regulates the anti-oxidant response by promoting the ubiquitination and proteasomal degradation of substrates, including the NRF2 transcription factor [4–7]. Oxidative and electrophilic stress induce cysteine modifications that disrupt KEAP1 function, allowing NRF2 to accumulate for the trans-activation of stress-response genes [8–10].

Ubiquitination by KEAP1 and other KLHL-family proteins is dependent on their binding to the N-terminal domain of CUL3 ($CUL3_{NTD}$), which acts as a scaffold for their assembly into multi-subunit Cullin-RING E3 ligases [11–15]. Following activation by an E1 enzyme, charged E2-ubiquitin conjugates are recruited to the E3 complex by the RING-domain containing RBX1 subunit, which assembles with the CUL3 *C*-terminal domain ($CUL3_{CTD}$) [16,17]. Neddylation of the $CUL3_{CTD}$ is predicted to induce conformational changes in the complex that position the ubiquitin moiety optimally for its conjugation to the KEAP1-bound substrate [18,19].

The structural basis for substrate recruitment by the Kelch domain of KEAP1 has been revealed by numerous co-crystal structures, including structures with both the 'ETGE' and 'DLG' degron motifs of NRF2 [20–27]. However, to date there are neither structures elucidating the critical interaction between KEAP1 and CUL3, nor data to show the

* Corresponding author.
** Corresponding author. Center for Systems Biology, Massachusetts General Hospital, Boston, MA, 02114, USA.
E-mail addresses: ralph@broadinstitute.org (R. Mazitschek), alex.bullock@cmd.ox.ac.uk (A.N. Bullock).
[1] These authors contributed equally to this work.
[2] Present address: Department of Molecular Biology and Genetics, Aarhus University, Denmark.

https://doi.org/10.1016/j.freeradbiomed.2023.04.021
Received 14 February 2023; Received in revised form 22 March 2023; Accepted 28 April 2023
Available online 6 May 2023

Abbreviations

BLI	biolayer interferometry
BTB	bric-à-brac, tramtrack and broad complex
BACK	BTB and *C*-terminal Kelch
CDDO	2-cyano-3,12-dioxooleana-1,9(11)-dien-28-oic acid
CI	confidence interval
DLG	Asp-Leu-Gly
ETGE	Glu-Thr-Gly-Glu
ITC	isothermal titration calorimetry
KEAP1	Kelch ECH associating protein 1
KLHL	Kelch-like
NRF2	Nuclear factor erythroid 2-related factor 2
Pfp	pentafluorophenyl
SCF	SKP1-CUL1-F-box
Tfp	Tetrafluorophenyl
TR-FRET	time-resolved Förster resonance energy transfer

contributions of different domains to their binding affinity. The molecular binding model (see schematic Fig. 1) is therefore currently inferred from the structures of other $CUL3_{NTD}$ complexes, including those of KLHL3 [28], KLHL11 [29], SPOP [30,31] and the vaccinia virus protein A55 [32], as well as the structure of the isolated BTB domain of KEAP1 [33]. Collectively, the structures identify a common interaction between the BTB domain and 3-box of the E3 and the first Cullin repeat domain of $CUL3_{NTD}$. The 3-box within the BACK domain forms a short helical motif that was found to be critical for high-affinity CUL3 interaction (analogous to the F-box and SOCS-boxes in other cullin-based E3s) [31]. The structure of the KLHL11-CUL3 complex showed the 3-box packing at the junction between the BTB and BACK domains, forming a hydrophobic groove that accommodated an N-terminal extension in CUL3 ('N22' in Fig. 1) [29]. Notably, deletion of the N-terminal extension resulted in a 30-fold lower affinity, highlighting its importance for the interaction [29].

Triterpenoid drugs, including 2-cyano-3,12-dioxooleana-1,9(11)-dien-28-oic acid (CDDO, bardoxolone), and its methyl ester CDDO-Me (bardoxolone methyl), have been postulated to restrict the interaction of KEAP1 with CUL3 and thereby stabilize NRF2 for cytoprotection [33,37]. This has led to the clinical investigation of CDDO-Me and analogs in conditions such as cancer, neurological disorders, chronic kidney disease, pulmonary hypertension and COVID-19, including omaveloxolone, which recently received FDA approval for the treatment of Friedreich's ataxia [5,38–43]. A co-crystal structure of CDDO revealed its covalent binding to Cys151 in a shallow pocket in the KEAP1 BTB domain [33], which we subsequently showed to bind reversibly with a K_D value of 3 nM [44]. However, from the crystallographic data, it remained unclear whether CDDO acts to restrict CUL3 binding – possibly via steric hindrance or via induced conformational changes [33]. Of note, a study utilizing fluorescence recovery after photobleaching (FRAP) in live cells did not establish support that CDDO abolishes KEAP1-CUL3 interaction, raising further uncertainty about the proposed mechanism of action [45]. There have also been conflicting reports on the stoichiometry of the KEAP1-CUL3 complex [46,47]. As the BTB domain of KEAP1 forms a homodimer, it is expected that the homodimer will afford binding sites for two CUL3 proteins (Fig. 1) [29,46]. However, at least one study has suggested that only one CUL3 protein is bound [47].

In this study, we aimed to provide a structural model of the KEAP1-CUL3 complex and to establish a robust assay system to measure their interaction affinity and the effect of CDDO. We determined a crystal structure of the BTB and 3-box domains of KEAP1 in complex with the $CUL3_{NTD}$ that revealed a heterotetrameric complex with a 2:2 stoichiometry. To support the structural data, we developed a generalizable TR-FRET-based assay system to profile the binding of BTB-domain-containing proteins to CUL3 and determine the contribution of distinct protein features, revealing the importance of the CUL3 N-terminal extension for high affinity binding. We further provide direct evidence that CDDO does not disrupt the KEAP1-CUL3 complex, even at high concentrations, but rather reduces the affinity of the KEAP1-CUL3 interaction.

2. Materials and methods

2.1. Constructs

For bacterial expression, human $KEAP1_{BTB\text{-}3\text{-}box}$ (Uniprot Q14145, residues 48–213) was cloned into the vector pNIC28-Bsa4, which

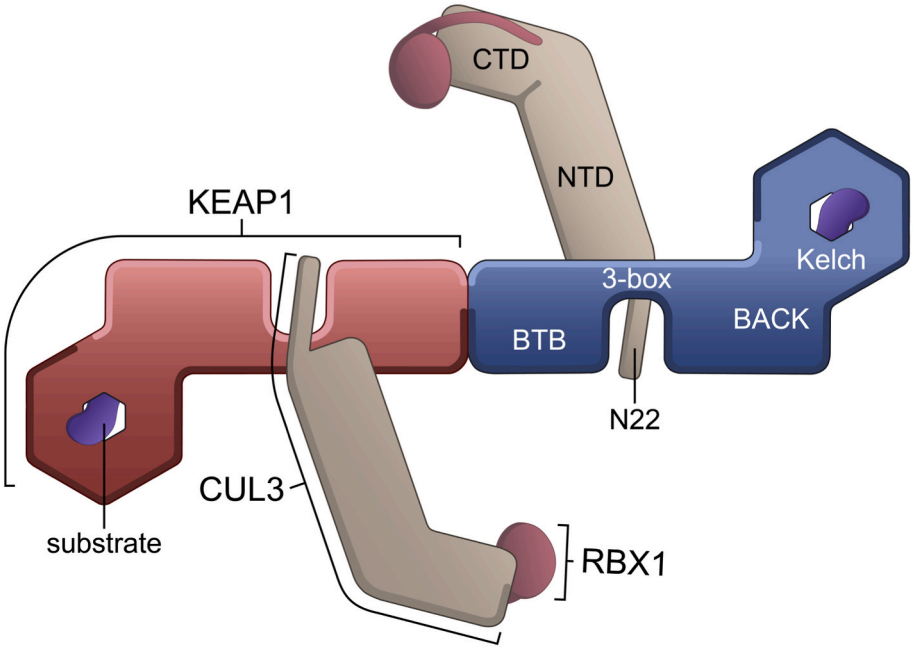

Fig. 1. Schematic showing the domain architecture of KEAP1 and CUL3 and predicted model for their interaction. KEAP1 is shown as a homodimer in red and blue. Substrate degrons (purple) are shown bound to the Kelch domains. The CUL3 (light brown) *C*-terminal domain (CTD) is bound to RBX1 (claret). The CUL3 N-terminal domain (NTD) and 22 residue N-terminal extension (N22) are predicted to bind to the KEAP1 BTB and 3-box domains (model based on the previously determined structure of a KLHL11-CUL3 complex [29]). The BTB domain was first identified as a conserved motif in the Drosophila proteins bric-à-brac, tramtrack and broad complex (reviewed in Ref. [34]). Likewise, the Kelch repeat domain was first identified in the Drosophila Kelch protein (reviewed in Ref. [35]). The BACK domain (for BTB and *C*-terminal Kelch) is also known as the intervening region (IVR) in KEAP1 and includes the 3-box motif at it N-terminus [36].

provides an N-terminal 6xHis tag with a TEV protease cleavage site. A further construct enabling biotinylation of $KEAP1_{BTB\text{-}3\text{-}box}$ was cloned into the pNIC-Bio3 vector, which provides a TEV-cleavable 6xHis tag and a *C*-terminal avi tag for biotinylation. Bacterial expression constructs for human $KLHL11_{BTB\text{-}BACK}$ (Q9NVR0, residues 67–340 in vector pNIC28-Bsa4), $CUL3_{NTD}$ (Q13618, residues 1–388 in pNIC-CTHF) and $CUL3_{NTD\Delta22}$ (residues 23–388 in pNIC-CTHF) were described previously [29]. Vector pNIC-CTHF provides *C*-terminal 6xHis and FLAG tags cleavable by TEV protease. A construct enabling biotinylation of $CUL3_{NTD}$ (residues 1–389) was cloned into the pNIC-Bio3 vector. All $CUL3_{NTD}$ constructs included mutations I342R and L346D designed to stabilize the isolated N-terminal domain (NTD) as part of the "split--n-express" strategy outlined by Zheng et al. [16].

For baculoviral expression, $KEAP1_{BTB\text{-}BACK\text{-}Kelch}$ (residues 48–624) and RBX1 (P62877 residues 1–108) were cloned into the baculoviral transfer vector pFB-LIC-Bse providing a TEV-cleavable N-terminal 6xHis tag. Full-length CUL3 (residues 1–768) was cloned into pFB-CT6HF-LIC, which provides *C*-terminal 6xHis and FLAG tags cleavable by TEV protease. Full-length KEAP1 was purchased from Sino Biological (cat# 11981-HNCB).

2.2. Protein expression and purification

Bacterial protein expression was performed in BL21(DE3)-pRARE2 cells. 2 L cultures were grown to mid-log phase in LB or 2xTY media with antibiotic selection, then cooled to 18 °C and induced with 0.25 mM IPTG. Cells were harvested by centrifugation and resuspended in 40 mL Binding Buffer (50 mM HEPES pH 7.5, 500 mM NaCl, 5% glycerol, 5 mM imidazole and 0.5 mM TCEP). Lysozyme (1 mg/mL), PEI (1 mL of 5% stock) and protease inhibitors were added before cell lysis by sonication. After centrifugation of the lysate at 50,000 g, the supernatant was filtered (1.2 μm) and incubated for 30 min with 3 mL nickel sepharose resin equilibrated in Binding Buffer. The column was washed with 50–80 mL Wash Buffer (50 mM HEPES pH 7.5, 500 mM NaCl, 5% glycerol, 30 mM imidazole and 0.5 mM TCEP) and the protein step eluted in 10 mL fractions of Binding Buffer supplemented with 50, 100, 150 and 250 mM imidazole. The fractions were pooled, diluted one third with Binding Buffer and cleaved overnight at 4 °C with tobacco etch virus (TEV) protease to remove the hexahistidine tags. Further purification was performed by size exclusion chromatography using on a 16/60 Superdex S200 column at 4 °C in Gel Filtration (GF) Buffer (50 mM HEPES pH 7.5, 300 mM NaCl, 0.5 mM TCEP). Peak fractions were pooled and concentrated with 10 mM DTT for storage or immediate use. For crystallography, $KEAP1_{BTB\text{-}3\text{-}box}$ and $CUL3_{NTD}$ were mixed in a 1:1 M ratio and incubated for 2 h on ice before the size exclusion chromatography step. For biotinylation, proteins were expressed in BL21(DE3)-pRARE2 cells containing a BirA co-expression vector and media supplemented with 100 μM D-biotin. An additional 10 mL of a 10 mM stock solution of D-biotin (prepared in 10 mM Bicine, pH 8.3 and filter sterilized) was added to the cell cultures 1 h before cell harvesting. Native and biotinylated protein masses were confirmed using intact mass spectrometry.

For baculoviral expression, plasmids were transformed into DH10Bac cells to generate bacmid DNA. Baculoviruses were then prepared from this using Sf9 insect cells. CUL3 and RBX1 viruses were co-infected to generate the CUL3-RBX1 complex, whereas $KEAP1_{BTB\text{-}BACK\text{-}Kelch}$ was prepared alone. Large-scale baculoviral expression was performed for 72 h at 27 °C. The harvested cells were resuspended in 40 mL binding buffer per 2L cell culture. PEI (1 mL) and protease inhibitors were added before cell lysis by sonication. After centrifugation of the lysate at 50,000 g, the supernatant was filtered and protein purified by nickel affinity and size exclusion chromatography as above.

2.3. Crystallisation

Crystallisation was achieved at 20 °C using the sitting drop vapour diffusion method. Initially, crystals grew in 0.1 M MMT, 0.2 M ammonium chloride, 15% PEG 3350, and diffracted to 6 Å. Further fine screening and seeding yielded plate-like crystals diffracting to 3.45 Å. The final protein complex crystallised at 9.4 mg/mL in 150 nL drops at a 1:2 ratio of protein to precipitant (20% PEG 3350, 10% ethylene glycol, 0.2 M potassium citrate tribasic), using an additional 20 nL of seeds previously prepared in a similar condition. Crystals were cryoprotected in 20% ethylene glycol in well precipitant and then vitrified in liquid nitrogen.

2.4. Structure determination

Diffraction data were collected at the Diamond Light Source, station I03 using monochromatic radiation at wavelength 0.97626 Å. Automated diffraction data reduction was performed using xia2 3d, and the indexed, integrated, scaled and merged data was phased using PhaserMR in Phenix [48] with a structure of $KLHL11_{BTB\text{-}BACK}$ complexed to $CUL3_{NTD}$ as the search model (PDB 4AP2). The molecular replacement (MR) structure solution was refined using Phenix [48] and Buster [49] with manual rebuilding with Coot [50]. Molprobity [51] was used to verify the geometrical correctness of the structure.

2.5. Biolayer interferometry

Biolayer interferometry (BLI) performed on an Octet RED384 instrument (FortéBio) was used to determine the binding affinity between different BTB-Kelch and CUL3 protein constructs as indicated. Biotinylated protein ligand buffered in 50 mM HEPES, 300 mM NaCl, 0.5 mM TCEP, and 10 mM DTT was used at 0.16 mg/mL to immobilise ligand onto streptavidin-coated fiber optic tips (FortéBio) to yield a binding response of 7–8 nm. Serial dilutions of the test analyte protein in the same buffer supplemented with 0.01% TWEEN-20 were placed in the relevant wells, with matching buffer in the reference wells. Association and dissociation phases were recorded as indicated. Steady-state equilibrium and kinetic fits were performed by global data analyses in the ForteBio Data Analysis 9.0 software using a 1:1 binding model.

2.6. TR-FRET measurements

Unless otherwise noted, experiments were performed in white, 384-well microtiter plates (Corning 3572) in 30 μL assay volume. TR-FRET measurements were acquired on a Tecan SPARK plate reader with SPARKCONTROL software version V2.1 (Tecan Group Ltd.), with the following settings: 340/50 nm excitation, 490/10 nm (Tb), and 520/10 nm (AF488) emission, 100 μs delay, 400 μs integration. The 490/10 nm and 520/10 nm emission channels were acquired with a 50% mirror and a dichroic 510 mirror, respectively, using independently optimized detector gain settings unless specified otherwise. The TR-FRET ratio was taken as the 520/490 nm intensity ratio on a per-well basis.

2.7. Protein labeling

Full-length KEAP1 (Sino Biological 11981-HNCB) and $KLHL11_{BTB\text{-}BACK}$ were labeled with CoraFluor-1-Pfp, and $CUL3_{NTD}$ was labeled with AF488-Tfp, as previously described [44]. The following extinction coefficients were used to calculate protein concentration and degree-of-labeling (DOL): KEAP1 $E_{280} = 80{,}335\ M^{-1}cm^{-1}$, KLHL11 $E_{280} = 34{,}295\ M^{-1}cm^{-1}$, $CUL3_{NTD}$ $E_{280} = 36{,}705\ M^{-1}cm^{-1}$, CoraFluor-1-Pfp $E_{340} = 22{,}000\ M^{-1}cm^{-1}$, AF488-Tfp $E_{495} = 71{,}000\ M^{-1}cm^{-1}$. Protein conjugates were snap-frozen in liquid nitrogen, and stored at −80 °C.

2.8. Determination of equilibrium dissociation constant (K_D) of AF488-labeled CUL3 toward CoraFluor-1-labeled KEAP1 and KLHL11

CoraFluor-1-labeled KEAP1 and KLHL11 were diluted to 1.5x (30 nM and 3 nM, respectively) in assay buffer (25 mM HEPES, 150 mM NaCl, 1

mM DTT, 0.5 mg/mL BSA, 0.005% TWEEN-20, pH 7.5). AF488-labeled $CUL3_{NTD}$ was added in serial dilution from 3x stock solutions in assay buffer (1:2 titration, 12-point, c_{max} = 1000 nM) and allowed to equilibrate for 2 h at room temperature before TR-FRET measurements were taken. Data were fitted to a One Site – Total Binding model in Prism 9.

2.9. Measurement of dissociation rate constants (k_{off}) by TR-FRET

Solutions of: (i) 20 nM CoraFluor-1-labeled KEAP1, 300 nM AF488-labeled $CUL3_{NTD}$, and (ii) 2 nM CoraFluor-1-labeled KLHL11, 45 nM AF488-labeled $CUL3_{NTD}$ were prepared in assay buffer and allowed to equilibrate for 2 h at room temperature before initial (t = 0) TR-FRET measurements were taken. Following addition of 25 μM unlabeled KLHL11, the time-dependent change of TR-FRET intensity was recorded (in 30 s intervals) over the course of 30 min. Data were normalized and fitted to a one-phase decay model in Prism 9.

2.10. TR-FRET protein displacement assays

The following assay parameters have been used (all 1.5x): (i) 30 nM CoraFluor-1-labeled KEAP1, 300 nM AF488-labeled $CUL3_{NTD}$ in assay buffer, (ii) 3 nM CoraFluor-1-labeled KLHL11, 45 nM AF488-labeled $CUL3_{NTD}$ in assay buffer. In all cases, protein constructs were added in serial dilution from 3x stock solutions in assay buffer (1:3 titration, 12-point, c_{max} = 25 μM) and allowed to equilibrate for 2 h at room temperature before TR-FRET measurements were taken. The assay floor (background) was defined with the 25 μM $CUL3_{NTD}$ dose, and the assay ceiling (top) was defined via a no-protein control. Data were background corrected, normalized, and fitted to a four-parameter dose-response model [log(inhibitor) vs. response – Variable slope (four parameters)] using Prism 9, with constraints of Top = 1, and Bottom = 0.

2.11. Calculation of protein K_D values from measured TR-FRET IC_{50}

For TR-FRET protein displacement assays, we have determined the K_D of the respective fluorescently labeled protein tracer under each assay condition. Protein K_D values have been calculated using Cheng-Prusoff principles, outlined in equation (1) below:

$$K_D = \frac{IC_{50}}{1 + \frac{[S]}{K_X}} \quad (1)$$

Where IC_{50} is the measured IC_{50} value, [S] is the concentration of the fluorescent protein tracer, and K_X is the K_D of the fluorescent protein tracer for a given condition [52].

3. Results

3.1. Structure determination

To determine the structural mechanisms of the KEAP1-CUL3 interaction, we prepared recombinant proteins with various truncations to identify regions compatible with crystallisation. Crystals were obtained following purification of a complex consisting of the BTB and 3-box regions of human KEAP1 (residues 48–213; herein $KEAP1_{BTB\text{-}3\text{-}box}$) and the N-terminal domain of CUL3 (residues 1–388; herein $CUL3_{NTD}$), consistent with the expected interaction domains (Fig. 1). Larger complexes comprising all folded domains of KEAP1 (residues 48–624, herein $KEAP1_{BTB\text{-}BACK\text{-}Kelch}$) or the full-length CUL3-RBX1 complex did not yield crystals in trials using 6 different sparse matrix crystal screens, perhaps reflecting their increased flexibility.

The resulting structure was solved by molecular replacement in space group C2 2 2_1 and refined at 3.45 Å resolution (see Table S1 for data collection and refinement statistics). A single chain each of KEAP1 and CUL3 was identified in the crystallographic asymmetric unit. The electron density maps allowed KEAP1 to be modelled from residues 51–204 and the CUL3 chain from residues 26–381, except for a disordered loop between residues 331 and 338. Crystallographic symmetry revealed the expected homodimerization of the KEAP1 BTB domain yielding an overall KEAP1-CUL3 heterotetrameric complex with a 2:2 stoichiometry and overall complex dimensions of 162 × 90 × 43 Å (Fig. 2).

3.2. Interactions in the KEAP1-CUL3 interface

The KEAP1 BTB and 3-box domains were bound exclusively to the first Cullin repeat domain of CUL3 (Fig. 3A). Compared to the free BTB structure [33], the KEAP1 BTB domain exhibited an induced fit characterized by alternative packing of the α3-β4 loop to insert KEAP1 Leu115 into a deep hydrophobic pocket formed between the H2 and H4 helices of CUL3 (Fig. 3A). Of note, Leu115 showed the highest buried interface area of any residue in the complex (Fig. 3B and C) and was displaced by 9 Å compared to the free KEAP1 structure (Fig. 3A). Leu115 belongs to a φ-x-E motif first defined in the SPOP-CUL3 structure, and conserved in BTB family E3 ligases [28,30], where Leu115 represents the hydrophobic residue φ, Arg116 is the charged/polar residue x and Glu117 is the conserved glutamate forming hydrogen bond interactions with the CUL3 H2 helix. The H2 and H5 helices of CUL3 are also notable for a cluster of tyrosine residues that form hydrogen bonds with the KEAP1 α5 and α7 helices in the BTB and 3-box domains, respectively (Fig. 3A). Superposition of the structure with the $KEAP1_{BTB}$-CDDO complex revealed that the CDDO binding site was on the opposite face of the BTB domain to the CUL3 interface and therefore was unlikely to directly disrupt these observed interactions (Fig. 3A).

3.3. Comparison with the extended interface of the KLHL11-CUL3 structure

Overall, the KEAP1-CUL3 interface buried a surface area of 833 $Å^2$. By comparison, the structure of a $KLHL11_{BTB\text{-}BACK}$ construct bound to $CUL3_{NTD}$ showed an extended interface of 1508 $Å^2$ boosted by additional interactions between an N-terminal CUL3 extension ("N22" in Fig. 1) and a hydrophobic groove formed between KLHL11 α5 (BTB) and α7 (3-box) (Fig. 4A and B) [29]. No electron density was observed for the same CUL3 N-terminal region in the KEAP1 complex despite the sequence similarity of the binding site (Fig. 4A). This might reflect hindrance from crystal packing (Fig. S1), or the absence of the full BACK domain in the crystallised KEAP1 construct, which is likely to stabilze the 3-box structure and form further minor contact with CUL3. In addition, the KEAP1 3-box contains some bulkier substitutions, such as Phe190, that could diminish the size of the hydrophobic groove for interaction (Fig. 4B). While the binding of the CUL3 N-terminal extension was not observed in the KEAP1 complex structure, modelling of this region using the equivalent $KLHL11_{BTB\text{-}BACK}$ co-structure suggested a potential steric clash between the CUL3 extension and the small molecule inhibitor CDDO (Fig. 4B), providing one possible explanation for its mode of action.

3.4. Biolayer interferometry indicates that $KEAP1_{BTB\text{-}3\text{-}box}$ binds to CUL3 relatively weakly

Next, we aimed to determine the binding affinity between KEAP1 and CUL3, and to evaluate the contributions of the CUL3 N-terminal extension, as well as the BTB-BACK and Kelch domains of KEAP1. We first used biolayer interferometry (BLI) to profile the interaction of the proteins used in the structure determination. Biotinylated $CUL3_{NTD}$ was captured on a streptavidin-functionalized sensor and binding was quantified using serial dilutions of $KEAP1_{BTB\text{-}3\text{-}box}$. The apparent K_D = 1.7 μM (95% CI 1.0–2.5 μM; Fig. 5) determined under steady-state conditions was comparable to the results obtained with a reverse setup immobilizing biotinylated $KEAP1_{BTB\text{-}3\text{-}box}$ and titrating serial dilutions of the $CUL3_{NTD}$ protein (Fig. S2A), or the full-length CUL3-RBX1

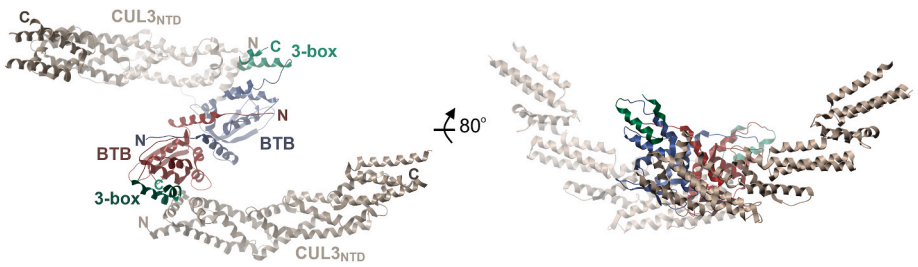

Fig. 2. Structure of the crystallised KEAP1-CUL3 complex. The structure shown in two orientations reveals a stoichiometry of 2:2 for $KEAP1_{BTB\text{-}3\text{-}box}$ binding to the $Cul3_{NTD}$.

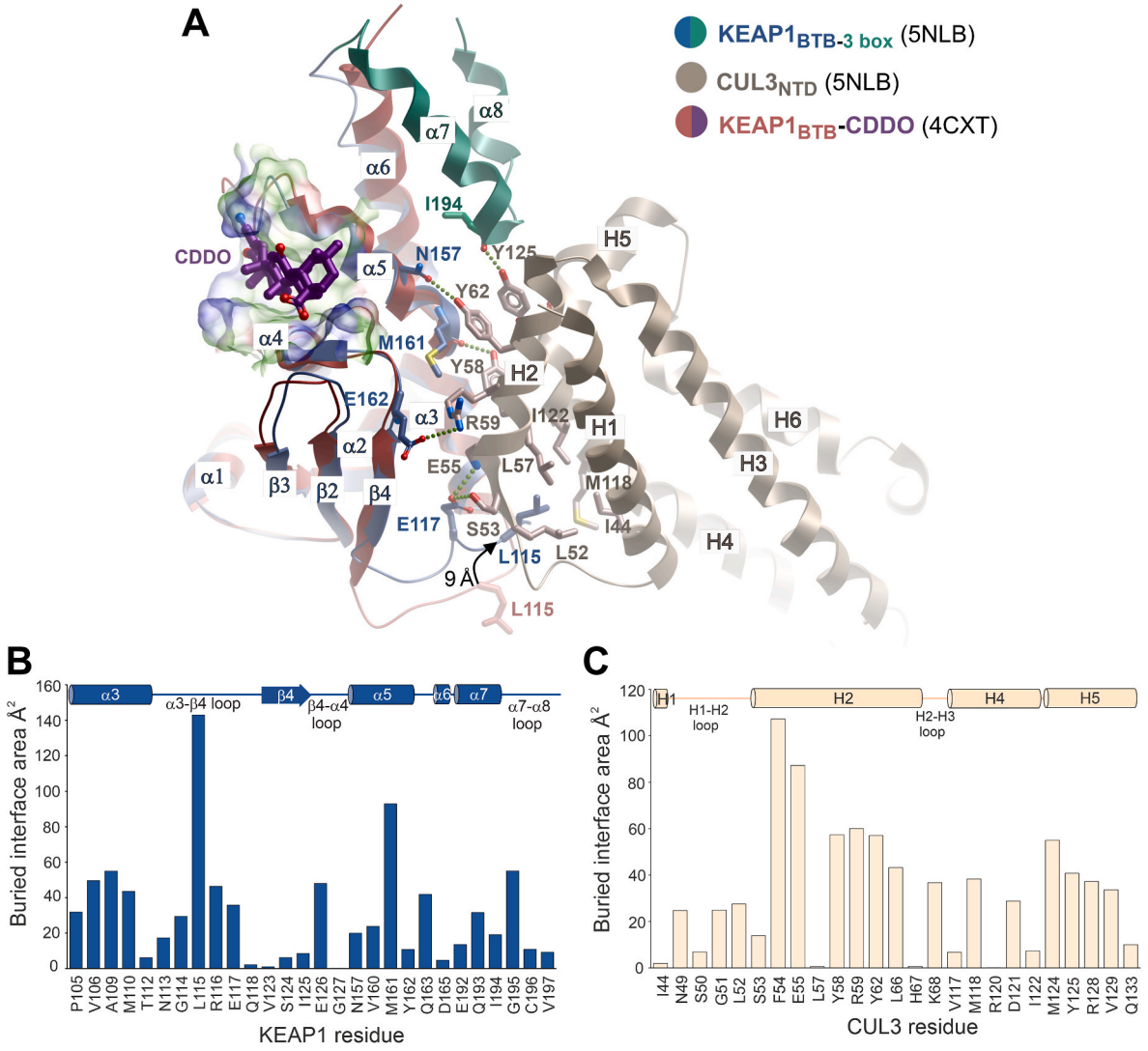

Fig. 3. Interactions in the KEAP1-CUL3 interface. (A) Superposition of the KEAP1-CUL3 complex with the previously determined structure of the KEAP1 BTB domain bound to CDDO. Different structural features are coloured according to the key. An arrow highlights conformational differences in the BTB α3-β4 loop in the two structures, as highlighted by the 9 Å difference in the position of KEAP1 Leu115. Selected hydrogen bonds (dotted lines) and hydrophobic interactions are shown in the KEAP1-CUL3 complex. A surface representation of the CDDO-binding pocket is shown with partial transparency. CDDO is shown as purple sticks. (B) Buried interface areas of KEAP1 residues bound to CUL3 calculated using the Protein interfaces, surfaces and assemblies service (PISA) at the European Bioinformatics Institute (http://www.ebi.ac.uk/pdbe/prot_int/pistart.html) [53]. Residue numbers and secondary structure elements are indicated. (C) Buried interface areas of CUL3 residues bound to KEAP1.

complex (Fig. S2B). The measured binding affinity was markedly weaker than those reported for $CUL3_{NTD}$ binding to $KLHL11_{BTB\text{-}BACK}$ (K_D = 20 nM [29]) or to a $SPOP_{BTB\text{-}3\text{-}box}$ construct (K_D = 17 nM [31]). Instead, the measured interaction was similar to previous studies using $CUL3_{NTD}$ constructs with an N-terminal deletion (either $CUL3_{NTD\Delta N19}$ or $CUL3_{NTD\Delta N22}$), including those analyzing binding to the SPOP BTB domain alone (K_D = 1.0 μM [30]), or to a lesser extent $KLHL11_{BTB\text{-}BACK}$ (K_D = 0.65 μM [29]) or $KLHL3_{BTB\text{-}BACK}$ (K_D = 0.11 μM [28]).

Together, these data highlight the importance of the interaction between the CUL3 N-terminal extension and the 3-box grove in BTB-

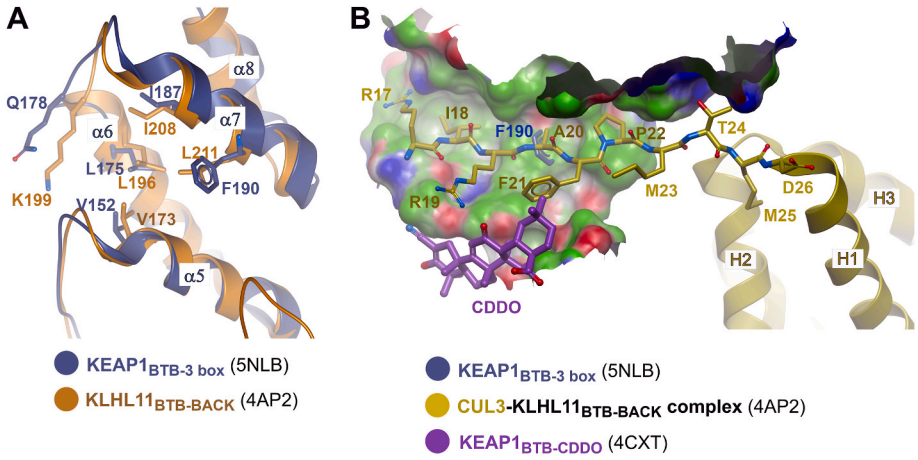

Fig. 4. Comparison of the 3-box hydrophobic groove in the respective KEAP1 and KLHL11 bound CUL3 complexes. (A) Superposition of KEAP1 (dark blue) and KLHL11 (orange) showing conservation of a hydrophobic groove between the BTB domain (α5) and 3 box (α7). KLHL11 Leu211 is replaced by Phe190 in KEAP1. (B) Superposition of CUL3 complexes of KEAP1 and KLHL11 with the KEAP1-CDDO complex. A surface representation of the 3-box hydrophobic groove in the KLHL11-CUL3 complex is shown (green with blue and red areas denoting hydrogen bond donor and acceptor positions, respectively) with interacting CUL3 residues shown as yellow sticks. Superposition predicts clashes between KEAP1 Phe190 (protruding through this surface) and CUL3 Ala20 as well as between KEAP1-bound CDDO and CUL3 Phe21.

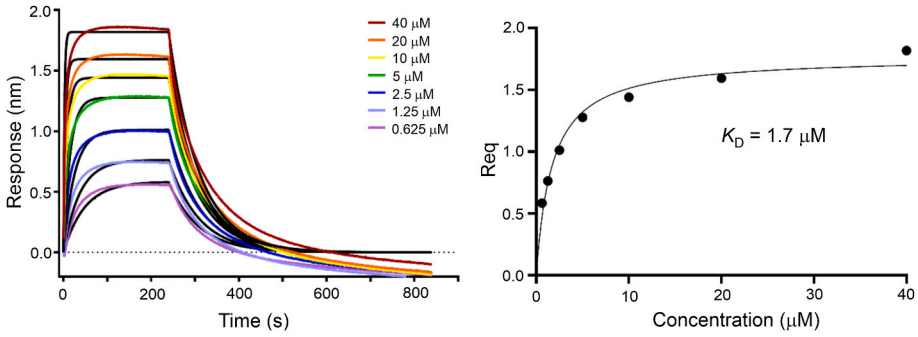

Fig. 5. Biolayer interferometry (BLI) measurements of CUL3 binding to the $KEAP1_{BTB\text{-}3\text{-}box}$. Binding equilibrium and kinetic measurements were determined on an Octet RED384 instrument (FortéBio). Biotinylated $CUL3_{NTD}$ was immobilized on a streptavidin-functionalized sensor tip and binding to serial dilutions of $KEAP1_{BTB\text{-}3\text{-}box}$ was quantified by fitting to a Langmuirian 1:1 model. Steady-state equilibrium analysis yielded an apparent K_D = 1.7 μM (95% CI 1.0–2.5 μM) and binding kinetics of $k_{on} = 1.02 \times 10^4\ M^{-1}s^{-1}$, $k_{off} = 1.45 \times 10^{-2}\ s^{-1}$, $^{App}K_D$ = 1.4 μM.

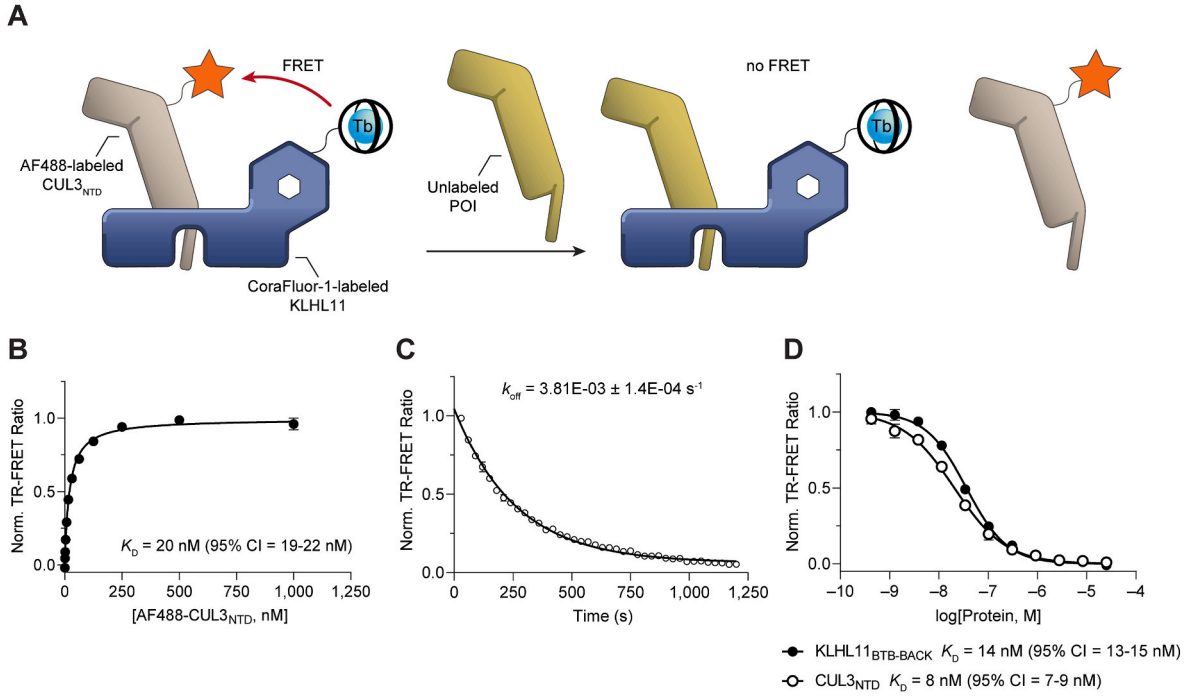

Fig. 6. Validation of TR-FRET assay approach with $KLHL11_{BTB\text{-}BACK}$ and $CUL3_{NTD}$. (A) Schematic of the TR-FRET assay principle with CoraFluor-1-labeled KLHL11 and AF488-labeled $CUL3_{NTD}$. Addition of unlabeled protein of interest (POI) competes with either $CUL3_{NTD}$ (shown) or KLHL11 (not shown), disrupting the TR-FRET process. For clarity, only one $KLHL11_{BTB\text{-}BACK\text{-}Kelch}$ subunit from the KLHL11 homodimer is shown. (B) Saturation binding of AF488-labeled $CUL3_{NTD}$ to CoraFluor-1-labeled $KLHL11_{BTB\text{-}BACK}$ yielded a K_D value of 20 nM, consistent with our previous ITC data [29]. (C) Determination of the dissociation rate constant ($k_{off} = 3.81 \times 10^{-3}\ s^{-1}$) establishes an assay equilibration time of ~15 min ($5 \times t_{1/2}$). (D) Dose-response titration of unmodified $KLHL11_{BTB\text{-}BACK}$ and $CUL3_{NTD}$ in TR-FRET protein displacement assay with AF488-labeled $CUL3_{NTD}$ and CoraFluor-1-labeled $KLHL11_{BTB\text{-}BACK}$.

containing proteins such as KLHL11 and SPOP. By extension, the lack of electron density for the CUL3 N-terminus in our co-structure with the $KEAP1_{BTB\text{-}3\text{-}box}$ may suggest the absence of this binding feature in KEAP1, providing a rationale for the comparatively low binding affinity measured with the KEAP1 constructs. To rule out that these results are not the consequences of the absence of a complete BACK domain, we set out to include $KEAP1_{BTB\text{-}BACK\text{-}Kelch}$ and an N-terminally truncated CUL3 that lacks all 3-box interacting residues ($CUL3_{NTD\Delta N22}$) in our analysis. Unfortunately, the $KEAP1_{BTB\text{-}BACK\text{-}Kelch}$ construct exhibited poor behavior in BLI experiments, precluding characterization of its binding to $CUL3_{NTD}$ (Fig. S2C). Similarly, we were unsuccessful in establishing a functional BLI assay for measuring the binding of $KEAP1_{BTB\text{-}3\text{-}box}$ to the $CUL3_{NTD\Delta N22}$ construct (Fig. S2D). We, therefore, explored a TR-FRET-based experimental design as an alternative strategy, following our previous work utilizing CoraFluor-1 as the luminescent donor for the characterization of KEAP1 ligands and KEAP1 homodimerization [44]. Homogenous TR-FRET assays offer several advantages over other biophysical methods and even enable the quantitative measurement of low-affinity interactions.

3.5. TR-FRET assays reveal the importance of other KEAP1 domains for CUL3 interaction

We rationalized that pairwise labeling of BTB-containing proteins and $CUL3_{NTD}$ would provide a straightforward and target-agnostic strategy for the characterization of binding affinities (Fig. 6A–D). TR-FRET donor and acceptor functionalization was accomplished through direct acylation using CoraFluor-1-Pfp and AF488-Tfp, respectively [54–56]. We selected direct chemical labeling over the use of labeled anti-epitope tag antibodies or streptavidin, which can complicate data interpretation due to the formation of higher-order complexes. To validate our approach, we first performed a saturation binding experiment with CoraFluor-1-labeled $KLHL11_{BTB\text{-}BACK}$ and AF488-$CUL3_{NTD}$, which yielded a K_D value of 20 nM (95% CI 19–22 nM), consistent with our previous ITC data (Fig. 6B) [29]. Direct measurement of the dissociation rate constant ($k_{off} = 3.81 \times 10^{-3}\ s^{-1}$) was determined by the addition of an excess of the respective unlabeled competitor to pre-equilibrated TR-FRET donor and acceptor functionalized protein complexes, establishing an assay equilibration time of ~15 min ($5 \times t_{1/2}$) (Fig. 6C) [57,58]. Dose-response titration of unlabeled $CUL3_{NTD}$ or $KLHL11_{BTB\text{-}BACK}$ as competitors yielded similar K_D values (Fig. 6D) and provided evidence that dye functionalization was well tolerated and did not alter the binding affinity (Table S2).

Because KEAP1 and KLHL11 bind to the same site of $CUL3_{NTD}$, this assay system is also suitable as a ligand displacement assay for profiling the binding affinity of KEAP1 constructs and, by extension, other BTB domain-containing proteins. However, some BTB proteins have previously been reported to form heterodimers, which could result in a non-linear response of this assay system and potentially misleading data [3]. Therefore, we first employed our previously reported KEAP1 dimerization assay to address this question and test the capacity of KLHL11 to form heterodimers with KEAP1 (Fig. S3) [44]. As shown in Fig. 7A, we did not observe KEAP1-KLHL11 heterodimerization, rendering our approach viable for the direct profiling of KEAP1--$CUL3_{NTD}$ interaction with this assay platform.

Next, we performed dose-response experiments with the respective KEAP1 constructs in the KLHL11-$CUL3_{NTD}$ protein displacement assay. We determined K_D values of 720 nM (95% CI 650–797 nM) and 798 nM (95% CI 730–882 nM) for $KEAP1_{BTB\text{-}3\text{-}box}$ and $KEAP1_{BTB\text{-}BACK\text{-}Kelch}$, respectively, suggesting that the complete BTB-BACK domain does not meaningfully contribute to the binding affinity of the KEAP1-$CUL3_{NTD}$ interaction compared to BTB-3-box alone (Fig. 7B). Notably, these results provide an absolute comparison of the respective binding affinities because the titrations of unlabeled KLHL11 and KEAP1 are performed with the same reporter system.

Following the validation of our assay approach, we developed a similar TR-FRET protein displacement assay using full-length, untagged KEAP1 ($KEAP1_{FL}$ residues 1–624) and $CUL3_{NTD}$ to establish a complete characterization of the KEAP1-$CUL3_{NTD}$ interaction. Saturation binding of CoraFluor-1-labeled $KEAP1_{FL}$ and AF488-labeled $CUL3_{NTD}$ yielded a K_D value of 222 nM (95% CI 211–234 nM; Fig. 8A), suggesting that the N-terminal 48 amino acids of KEAP1 may contribute to higher affinity KEAP1-$CUL3_{NTD}$ binding. Kinetic analysis provided a k_{off}-value of $5.04 \times 10^{-3}\ s^{-1}$ (assay equilibration time ~12 min; Fig. 8B), and dose-response titration of $KEAP1_{BTB\text{-}3\text{-}box}$ and $KEAP1_{BTB\text{-}BACK\text{-}Kelch}$ yielded similar affinity values as measured in our orthogonal assay ($K_D = 1042$ nM [95% CI 943–1151 nM] and 396 nM [95% CI 363–430 nM], respectively) (Fig. 8C, Table S3). All further experiments were performed with the full-length, untagged KEAP1 for physiological relevance.

To assess the relevance of the N-terminal extension in CUL3, we employed our suite of TR-FRET protein displacement assays to characterize the affinity of $CUL3_{NTD\Delta22}$ for both $KEAP1_{FL}$ and $KLHL11_{BTB\text{-}BACK}$ (Fig. 9). We found that the lack of the N-terminus in CUL3 decreased the affinity for $KLHL11_{BTB\text{-}BACK}$ by > 200-fold ($K_D = 1840$ nM [95% CI 1702-1990 nM]), which is even more pronounced than the 30-fold reduction estimated by ITC in our previous report [29]. Similarly, we observed a ~100-fold decreased affinity of $KEAP1_{FL}$ for $CUL3_{NTD\Delta22}$ ($K_D = 13{,}783$ nM [95% CI 12,047-16,119 nM]) compared with $CUL3_{NTD}$ ($K_D = 129$ nM [95% CI 117–142 nM]). This result was unexpected because of the lack of electron density for the 22 amino acid N-terminal extension in our $KEAP1_{BTB\text{-}3\text{-}box}$-$CUL3_{NTD}$ co-crystal structure. Nonetheless, our data support the role of the N-terminus in mediating high-affinity interactions between the KEAP1/KLHL11 3-box grooves and CUL3, and suggest that the complete BACK domain might be required for structured binding.

3.6. TR-FRET reveals partial inhibition by CDDO

We have previously shown that CDDO binds to the KEAP1 BTB with

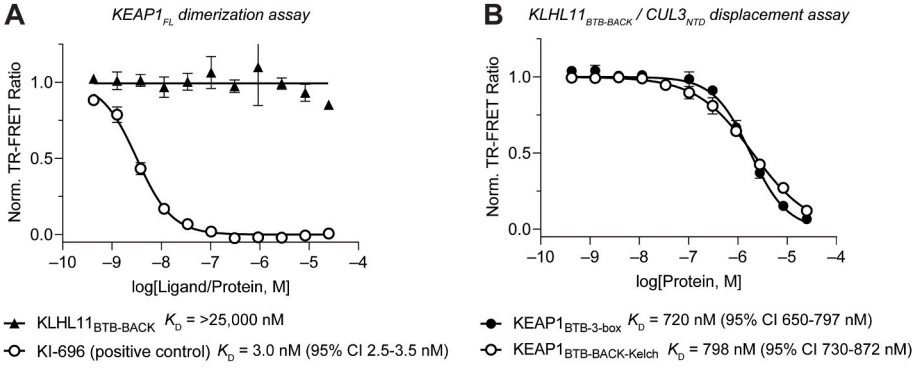

Fig. 7. A generalizable TR-FRET platform for profiling BTB domain-containing proteins. (A) Dose-response titration of $KLHL11_{BTB\text{-}BACK}$ and small molecule KEAP1-Kelch domain inhibitor KI-696 (positive control) in $KEAP1_{FL}$ dimerization assay [44,59], using a mixture of CoraFluor-1- and FITC-labeled Nrf2-derived peptides (LDEETGEFL--$CONH_2$), showing that $KLHL11_{BTB\text{-}BACK}$ does not heterodimerize with $KEAP1_{FL}$ at concentrations up to 25 μM. Also see Fig. S3 (B) Dose-response titration of $KEAP1_{BTB\text{-}3\text{-}box}$ and $KEAP1_{BTB\text{-}BACK\text{-}Kelch}$ in $KLHL11_{BTB\text{-}BACK}$-$CUL3_{NTD}$ TR-FRET protein displacement assay provides evidence that the complete BTB-BACK domain does not meaningfully contribute to the binding affinity of the KEAP1-$CUL3_{NTD}$ interaction.

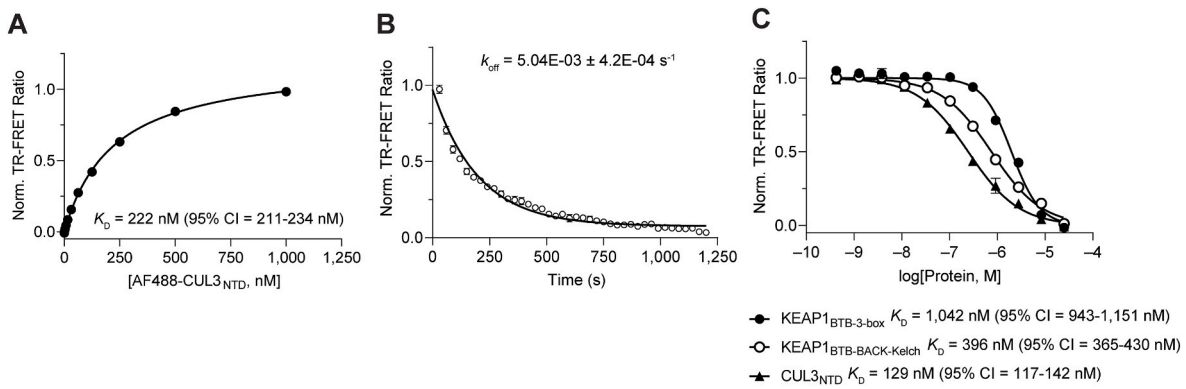

Fig. 8. KEAP1$_{FL}$-CUL3$_{NTD}$ TR-FRET protein displacement assay further characterizes KEAP1-CUL3NTD interaction. (A) Saturation binding of AF488-labeled CUL3$_{NTD}$ to CoraFluor-1-labeled KEAP1$_{FL}$ yielded a K_D value of 222 nM, suggesting that the N-terminal 48 residues of KEAP1$_{FL}$ contribute to slightly higher binding affinity to CUL3$_{NTD}$. (B) k_{off} determination (koff = 5.04 × 10^{-3} s^{-1}) establishes an assay equilibration time of ~12 min (5 × $t_{1/2}$). (C) Dose-response titration of unmodified KEAP1$_{BTB-3-box}$, KEAP1$_{BTB-BACK-Kelch}$, and CUL3$_{NTD}$ in TR-FRET protein displacement assay with AF488-labeled CUL3$_{NTD}$ and CoraFluor-1-labeled KEAP1$_{FL}$.

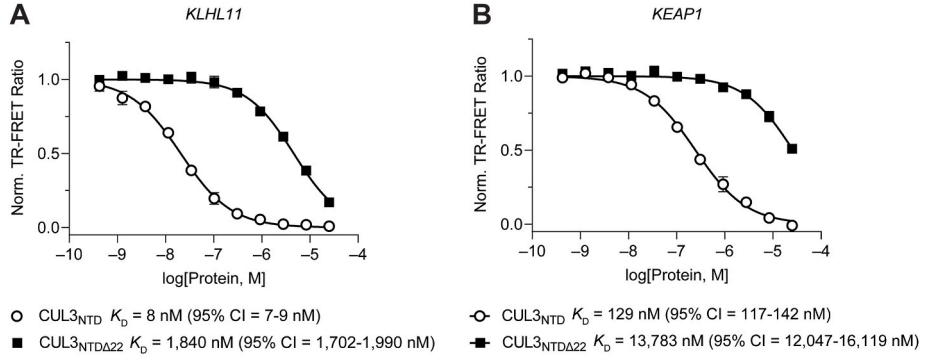

Fig. 9. Examining the role of the CUL3$_{NTD}$ N-terminal extension on binding affinity toward KLHL11 and KEAP1. (A–B) Dose-response titration of CUL3$_{NTD}$ and CUL3$_{NTDΔ22}$ in TR-FRET protein displacement assay between AF488-labeled CUL3$_{NTD}$ and (A) CoraFluor-1-labeled KLHL11$_{BTB-BACK}$, or (B) CoraFluor-1-labeled KEAP1$_{FL}$. Deletion of the N-terminal 22 amino acid residues results in a ~100-fold loss of binding affinity of CUL3$_{NTD}$ toward both proteins.

K_D = 3 nM but does not interfere with KEAP1 dimerization [44]. To understand if CDDO can inhibit KEAP1-CUL3 complex formation, we used our TR-FRET platform and evaluated CDDO in dose response. We found a dose-dependent decrease in signal intensity that plateaued at 50% "inhibition" at high compound concentrations (Fig. 10A). Although this type of "incomplete" inhibition can be observed for small molecules that are insufficiently soluble at concentrations above the IC$_{50}$ in the respective assay system, this is not the case for CDDO. An alternative explanation for this observation is that CDDO binding alters the affinity between KEAP1 and CUL3. We, therefore, determined the binding affinity of KEAP1$_{FL}$ to CUL3$_{NTD}$ in the absence and presence of high concentrations of CDDO. The saturation binding experiments revealed that CDDO decreases KEAP1-CUL3$_{NTD}$ binding affinity by > 2-fold, functioning only as a partial antagonist that cannot completely disrupt the complex (Fig. 10B). Although this shift in affinity might be sufficient to modulate the function of this critical redox sensor in cells to trigger activation of the ARE (anti-oxidant response element), it does not rule out more pronounced functional consequences as the result of a

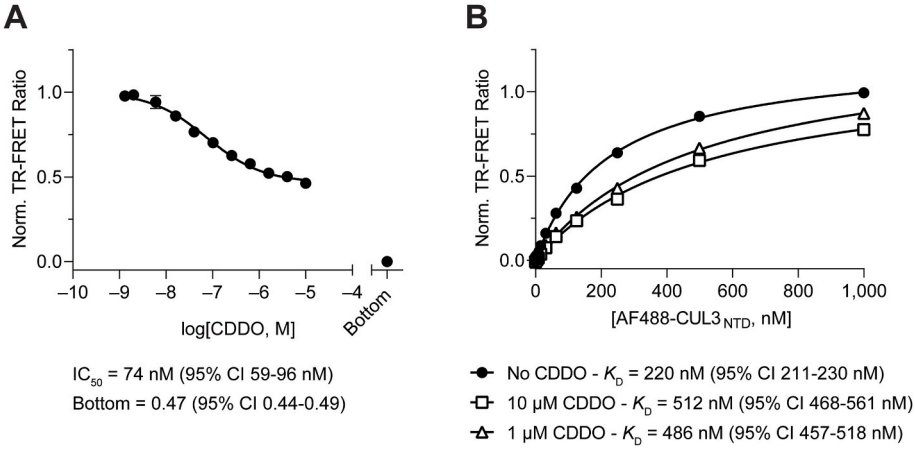

Fig. 10. CDDO is a partial antagonist of the KEAP1-CUL3 interaction. (A) Dose-response titration of CDDO in protein displacement assay with AF488-labeled CUL3$_{NTD}$ and CoraFluor-1-labeled KEAP1$_{FL}$ yielded an IC$_{50}$ value of 74 nM and incomplete inhibition. Assay floor was determined with 25 μM CUL3$_{NTD}$. (B) Saturation binding of AF488-labeled CUL3$_{NTD}$ to CoraFluor-1-labeled KEAP1$_{FL}$ in the absence or presence of 1 or 10 μM CDDO reveals that CUL3$_{NTD}$ has >2-fold reduced affinity toward the KEAP1-CDDO binary complex compared to KEAP1 alone.

distorted orientation of CUL3 with respect to the protein substrate.

4. Discussion

Cullin-RING ligase complexes typically utilize separate protein subunits as Cullin adaptor and substrate receptor. For example, the SCF (SKP1-CUL1-F-box) class use SKP1 as an adaptor to link CUL1 with an F-box-containing protein that functions as the substrate receptor [16]. CUL3 complexes form an exception in which both functionalities are incorporated into a single protein (e.g. KEAP1), allowing greater sequence diversity in their Cullin interfaces [29,60]. While the sequences of the KEAP1 BTB and 3-box domains have diverged from other BTB-containing proteins (e.g. 26.5% sequence identity across these domains in KLHL11), their structure in complex with $CUL3_{NTD}$ shows a conserved mechanism of assembly, including a heterotetrameric packing arrangement with 2:2 stoichiometry and an induced fit of the KEAP1 α3-β4 loop.

Except for KLHL11, all previously determined co-structures used truncated forms of CUL3 lacking the N-terminal extension. Thus, in our new structure of the KEAP1-CUL3 complex, we expected to observe the packing of the N-terminal CUL3 region ('N22'), similar to the KLHL11 co-structure, that would provide a better understanding of the predicted interaction with the 3-box groove and establish a molecular basis for the antagonistic effects of CDDO. However, this region appears to be disordered in the new structure, with the first defined CUL3 residue (Asp26) located some 19 Å from the CDDO binding site, where its interaction with KEAP1 is unlikely to be affected. The 3-box groove appears to be slightly shallower in KEAP1 than in KLHL11. Cleasby et al. previously postulated that the CUL3 N-terminal extension might instead bind to the KEAP1 Cys151 site and therefore compete more directly with CDDO [33]. However, our structure provides no evidence to support this prediction. Nonetheless, in agreement with Cleasby et al., we observe a potential steric clash with CUL3 when modelling its binding to the 3-box groove. To gain insights into the contributions of different domains and the impact of CDDO on KEAP1-CUL3 binding, we determined the equilibrium binding constants and binding kinetics of the various constructs. Unfortunately, we were unable to establish functional biolayer interferometry assays for several protein combinations. However, we successfully developed a robust and versatile biochemical TR-FRET assay platform based on our CoraFluor technology that facilitated the comprehensive, quantitative measurement of the CUL3 interactions. Importantly, when available, the data obtained by TR-FRET were in good agreement with the results determined by BLI.

Although the CUL3 N-terminal extension was not defined in the electron density maps of the KEAP1-CUL3 complex, its deletion still resulted in >100-fold loss of affinity, demonstrating its importance for the interaction. Notably, this affinity differential is comparable to the results obtained for KLHL11-CUL3, for which the CUL3 N-terminal extension is well-refined in the co-complex structure. However, it should be noted that KLHL11 binds significantly (~10-fold) tighter to the CUL3 constructs than KEAP1. Additionally, we observed a modest contribution to the binding affinity in the presence of the KEAP1 full N-terminus and Kelch domain, as apparent by the comparison of full-length and truncated KEAP1 ($K_{D,full\text{-}length}$ ~ 0.2 μM vs. $K_{D,BTB\text{-}3\text{-}box}$ ~1 μM), which might be the consequence of more stable folding of the BTB and 3-box domains within the full-length protein.

Furthermore, our TR-FRET assay approach also allowed us to examine the effect of CDDO on KEAP1-CUL3 binding. The KEAP1-CUL3 module has been recognized as a primary target of the cysteine-reactive oleanolic acid derivative CDDO and its analogs. However, the precise mechanism of how CDDO interferes with the function of KEAP1-CUL3 has still not been completely understood. It has previously been shown by crystallography that CDDO binds covalently to Cys151 within the BTB domain of KEAP1 [33]. Based on this and other observations, various modes of action have been proposed, including the disruption of KEAP1 dimer formation and inhibition of KEAP1-CUL3 binding [33, 61–63]. Our recent studies showed that CDDO does not disrupt KEAP1 dimerization [44]. Here, we further demonstrated that CDDO does not disrupt KEAP1-CUL3 binding in agreement with cellular binding studies [45,64]. Instead, we found that CDDO can act as a partial antagonist that appears to lower the affinity of CUL3 for KEAP1, but does not block the binding of the two proteins. Our findings are consistent with CDDO acting as an allosteric competitive inhibitor that interferes with binding of the CUL3 N-terminal domain to the 3-box groove of KEAP1, which we have shown significantly contributes to the binding affinity of CUL3 and KEAP1. Although we cannot rule out an alternative mechanism. The reversible addition of CDDO or CDDO-me on the thiol of KEAP1 Cys151 has not been detected by mass spectrometry, nor on any other residue within the full length protein [65,66]. Irreversible binding of the analog CDDO-epoxide has been mapped to KEAP1 cysteines at positions 257, 273, 288, 434, 489, and 613, both in vitro and in living cells, which could affect multiple protein-protein interactions, although its distinct chemistry could alter its reactivity and selectivity [65]. Thus, at higher concentrations, it is remains possible that CDDO derivatives might be binding to other Cys-side chains of KEAP1 (and/or CUL3), causing structural changes to alter the binding affinity (similar to the absence of the complete N- and *C*-termini of KEAP1). However, further studies will be needed to explore this activity in greater detail.

Together, the presented structural and biochemical data show the importance of the modular domains of KEAP1 and CUL3 for their heteromeric assembly. KEAP1 represents only one of nearly 200 BTB-containing proteins that can potentially assemble with CUL3 [67]. The established TR-FRET assay system offers a generalizable platform for profiling this protein class and may form a suitable screening platform for ligands that disrupt these interactions by targeting the BTB or 3-box domains to block E3 ligase function.

Data availability

The atomic coordinates and structure factors have been deposited in the Protein Data Bank, Research Collaboratory for Structural Bioinformatics, Rutgers University, New Brunswick, NJ (http://www.rcsb.org/) with PDB code 5NLB.

Author contributions

R.J.A. prepared recombinant proteins, performed the final crystallography, solved the structure and performed the biolayer interferometry. S.G.B. conducted initial crystal screens and protein production. N. C.P performed the TR-TRET experiments. R.J.A., N.C.P., R.M. and A.N.B. contributed to data analysis and manuscript preparation. R.M. and A.N. B helped with supervision and study design. All authors approved the final manuscript.

Funding

This research was supported by the CHDI Foundation to R.J.A., S.G. B. and A.N.B. A.N.B. also acknowledges funding from the Innovative Medicines Initiative 2 Joint Undertaking (JU) under grant agreement No 875510 (EUbOPEN). The JU receives support from the European Union's Horizon 2020 research and innovation programme and EFPIA and Ontario Institute for Cancer Research, Royal Institution for the Advancement of Learning McGill University, Kungliga Tekniska Hoegskolan, Diamond Light Source Limited. R.J.A. and A.N.B. also received support from the SGC (charity no. 1097737) which received funds from AbbVie, Bayer Pharma AG, Boehringer Ingelheim, Canada Foundation for Innovation, Eshelman Institute for Innovation, Genome Canada, Innovative Medicines Initiative (EU/EFPIA) [ULTRA-DD grant no. 115766], Janssen, Merck KGaA Darmstadt Germany, MSD, Novartis Pharma AG, Ontario Ministry of Economic Development and Innovation, Pfizer, Saõ Paulo Research Foundation-FAPESP, Takeda, and Wellcome [106169/ZZ14/Z]. This work was further supported by NSF

1830941 to R.M. N.C.P. was supported by a National Science Foundation Graduate Research Fellowship (DGE1745303).

Declaration of competing interest

R.M. is a scientific advisory board (SAB) member and equity holder of Regenacy Pharmaceuticals, ERX Pharmaceuticals, and Frequency Therapeutics. R.M. and N.C.P. are inventors on patent applications related to the CoraFluor TR-FRET probes used in this work.

Acknowledgments

The authors would like to thank Diamond Light Source for beamtime (proposal mx10619), as well as the staff of beamline I03 for assistance with crystal testing and data collection. We also thank David A Cruz Walma for help with the schematic in Fig. 1.

Appendix A. Supplementary data

Supplementary data to this article can be found online at https://doi.org/10.1016/j.freeradbiomed.2023.04.021.

References

[1] X. Shi, S. Xiang, J. Cao, H. Zhu, B. Yang, Q. He, M. Ying, Kelch-like proteins: physiological functions and relationships with diseases, Pharmacol. Res. 148 (2019), 104404.
[2] G. Ye, J. Wang, W. Yang, J. Li, M. Ye, X. Jin, The roles of KLHL family members in human cancers, Am. J. Cancer Res 12 (11) (2022) 5105–5139.
[3] E.L. Mena, R.A.S. Kjolby, R.A. Saxton, A. Werner, B.G. Lew, J.M. Boyle, R. Harland, M. Rape, Dimerization quality control ensures neuronal development and survival, Science 362 (6411) (2018), eaap8236.
[4] H. Panda, H. Wen, M. Suzuki, M. Yamamoto, Multifaceted roles of the KEAP1-NRF2 system in cancer and inflammatory disease milieu, Antioxidants 11 (3) (2022) 538.
[5] A. Cuadrado, A.I. Rojo, G. Wells, J.D. Hayes, S.P. Cousin, W.L. Rumsey, O. C. Attucks, S. Franklin, A.L. Levonen, T.W. Kensler, A.T. Dinkova-Kostova, Therapeutic targeting of the NRF2 and KEAP1 partnership in chronic diseases, Nat. Rev. Drug Discov. 18 (4) (2019) 295–317.
[6] A. Kobayashi, M.I. Kang, H. Okawa, M. Ohtsuji, Y. Zenke, T. Chiba, K. Igarashi, M. Yamamoto, Oxidative stress sensor Keap1 functions as an adaptor for Cul3-based E3 ligase to regulate proteasomal degradation of Nrf2, Mol. Cell Biol. 24 (16) (2004) 7130–7139.
[7] Y. Zhang, Z. Shi, Y. Zhou, Q. Xiao, H. Wang, Y. Peng, Emerging substrate proteins of kelch-like ECH associated protein 1 (Keap1) and potential challenges for the development of small-molecule inhibitors of the keap1-nuclear factor erythroid 2-related factor 2 (Nrf2) protein-protein interaction, J. Med. Chem. 63 (15) (2020) 7986–8002.
[8] K. Itoh, T. Chiba, S. Takahashi, T. Ishii, K. Igarashi, Y. Katoh, T. Oyake, N. Hayashi, K. Satoh, I. Hatayama, M. Yamamoto, Y. Nabeshima, An Nrf2/small Maf heterodimer mediates the induction of phase II detoxifying enzyme genes through antioxidant response elements, Biochem. Biophys. Res. Commun. 236 (2) (1997) 313–322.
[9] S. Dayalan Naidu, A.T. Dinkova-Kostova, KEAP1, a cysteine-based sensor and a drug target for the prevention and treatment of chronic disease, Open Biol. 10 (6) (2020), 200105.
[10] C.E. Badr, C.C. da Hora, A.B. Kirov, E. Tabet, R. Amante, S. Maksoud, A.E. Nibbs, E. Fitzsimons, M. Boukhali, J.W. Chen, N.H.L. Chiu, I. Nakano, W. Haas, R. Mazitschek, B.A. Tannous, Obtusaquinone: a cysteine-modifying compound that targets Keap1 for degradation, ACS Chem. Biol. 15 (6) (2020) 1445–1454.
[11] L. Xu, Y. Wei, J. Reboul, P. Vaglio, T.H. Shin, M. Vidal, S.J. Elledge, J.W. Harper, BTB proteins are substrate-specific adaptors in an SCF-like modular ubiquitin ligase containing CUL-3, Nature 425 (6955) (2003) 316–321.
[12] M. Furukawa, Y.J. He, C. Borchers, Y. Xiong, Targeting of protein ubiquitination by BTB-Cullin 3-Roc1 ubiquitin ligases, Nat. Cell Biol. 5 (11) (2003) 1001–1007.
[13] R. Geyer, S. Wee, S. Anderson, J. Yates, D.A. Wolf, BTB/POZ domain proteins are putative substrate adaptors for cullin 3 ubiquitin ligases, Mol. Cell. 12 (3) (2003) 783–790.
[14] M. McMahon, K. Itoh, M. Yamamoto, J.D. Hayes, Keap1-dependent proteasomal degradation of transcription factor Nrf2 contributes to the negative regulation of antioxidant response element-driven gene expression, J. Biol. Chem. 278 (24) (2003) 21592–21600.
[15] M. Furukawa, Y. Xiong, BTB protein Keap1 targets antioxidant transcription factor Nrf2 for ubiquitination by the Cullin 3-Roc1 ligase, Mol. Cell Biol. 25 (1) (2005) 162–171.
[16] N. Zheng, B.A. Schulman, L. Song, J.J. Miller, P.D. Jeffrey, P. Wang, C. Chu, D. M. Koepp, S.J. Elledge, M. Pagano, R.C. Conaway, J.W. Conaway, J.W. Harper, N. P. Pavletich, Structure of the Cul1-Rbx1-Skp1-F boxSkp2 SCF ubiquitin ligase complex, Nature 416 (6882) (2002) 703–709.
[17] J.W. Harper, B.A. Schulman, Cullin-RING ubiquitin ligase regulatory circuits: a quarter century beyond the F-box hypothesis, Annu. Rev. Biochem. 90 (2021) 403–429.
[18] D.M. Duda, L.A. Borg, D.C. Scott, H.W. Hunt, M. Hammel, B.A. Schulman, Structural insights into NEDD8 activation of cullin-RING ligases: conformational control of conjugation, Cell 134 (6) (2008) 995–1006.
[19] K. Baek, D.T. Krist, J.R. Prabu, S. Hill, M. Klugel, L.M. Neumaier, S. von Gronau, G. Kleiger, B.A. Schulman, NEDD8 nucleates a multivalent cullin-RING-UBE2D ubiquitin ligation assembly, Nature 578 (7795) (2020) 461–466.
[20] S.C. Lo, X. Li, M.T. Henzl, L.J. Beamer, M. Hannink, Structure of the Keap1:Nrf2 interface provides mechanistic insight into Nrf2 signaling, EMBO J. 25 (15) (2006) 3605–3617.
[21] B. Padmanabhan, K.I. Tong, T. Ohta, Y. Nakamura, M. Scharlock, M. Ohtsuji, M. I. Kang, A. Kobayashi, S. Yokoyama, M. Yamamoto, Structural basis for defects of Keap1 activity provoked by its point mutations in lung cancer, Mol. Cell. 21 (5) (2006) 689–700.
[22] T. Fukutomi, K. Takagi, T. Mizushima, N. Ohuchi, M. Yamamoto, Kinetic, thermodynamic, and structural characterizations of the association between Nrf2-DLGex degron and Keap1, Mol. Cell Biol. 34 (5) (2014) 832–846.
[23] B. Padmanabhan, Y. Nakamura, S. Yokoyama, Structural analysis of the complex of Keap1 with a prothymosin alpha peptide, Acta Crystallogr., Sect. F: Struct. Biol. Cryst. Commun. 64 (Pt 4) (2008) 233–238.
[24] M. Komatsu, H. Kurokawa, S. Waguri, K. Taguchi, A. Kobayashi, Y. Ichimura, Y. S. Sou, I. Ueno, A. Sakamoto, K.I. Tong, M. Kim, Y. Nishito, S. Iemura, T. Natsume, T. Ueno, E. Kominami, H. Motohashi, K. Tanaka, M. Yamamoto, The selective autophagy substrate p62 activates the stress responsive transcription factor Nrf2 through inactivation of Keap1, Nat. Cell Biol. 12 (3) (2010) 213–223.
[25] Y. Ichimura, S. Waguri, Y.S. Sou, S. Kageyama, J. Hasegawa, R. Ishimura, T. Saito, Y. Yang, T. Kouno, T. Fukutomi, T. Hoshii, A. Hirao, K. Takagi, T. Mizushima, H. Motohashi, M.S. Lee, T. Yoshimori, K. Tanaka, M. Yamamoto, M. Komatsu, Phosphorylation of p62 activates the Keap1-Nrf2 pathway during selective autophagy, Mol. Cell. 51 (5) (2013) 618–631.
[26] L.J. Beamer, X. Li, C.A. Bottoms, M. Hannink, Conserved solvent and side-chain interactions in the 1.35 Angstrom structure of the Kelch domain of Keap1, Acta Crystallogr. D Biol. Crystallogr. 61 (Pt 10) (2005) 1335–1342.
[27] X. Li, D. Zhang, M. Hannink, L.J. Beamer, Crystal structure of the Kelch domain of human Keap1, J. Biol. Chem. 279 (52) (2004) 54750–54758.
[28] A.X. Ji, G.G. Prive, Crystal structure of KLHL3 in complex with Cullin3, PLoS One 8 (4) (2013), e60445.
[29] P. Canning, C.D.O. Cooper, T. Krojer, J.W. Murray, A.C.W. Pike, A. Chaikuad, T. Keates, C. Thangaratnarajah, V. Hojzan, B.D. Marsden, O. Gileadi, S. Knapp, F. von Delft, A.N. Bullock, Structural basis for Cul3 protein assembly with the BTB-Kelch family of E3 ubiquitin ligases, J. Biol. Chem. 288 (11) (2013) 7803–7814.
[30] W.J. Errington, M.Q. Khan, S.A. Bueler, J.L. Rubinstein, A. Chakrabartty, G. G. Prive, Adaptor protein self-assembly drives the control of a cullin-RING ubiquitin ligase, Structure 20 (7) (2012) 1141–1153.
[31] M. Zhuang, M.F. Calabrese, J. Liu, M.B. Waddell, A. Nourse, M. Hammel, D. J. Miller, H. Walden, D.M. Duda, S.N. Seyedin, T. Hoggard, J.W. Harper, K. P. White, B.A. Schulman, Structures of SPOP-substrate complexes: insights into molecular architectures of BTB-Cul3 ubiquitin ligases, Mol. Cell. 36 (1) (2009) 39–50.
[32] C. Gao, M.A. Pallett, T.I. Croll, G.L. Smith, S.C. Graham, Molecular basis of cullin-3 (Cul3) ubiquitin ligase subversion by vaccinia virus protein A55, J. Biol. Chem. 294 (16) (2019) 6416–6429.
[33] A. Cleasby, J. Yon, P.J. Day, C. Richardson, I.J. Tickle, P.A. Williams, J.F. Callahan, R. Carr, N. Concha, J.K. Kerns, H. Qi, T. Sweitzer, P. Ward, T.G. Davies, Structure of the BTB domain of Keap1 and its interaction with the triterpenoid antagonist CDDO, PLoS One 9 (6) (2014), e98896.
[34] P.J. Stogios, G.S. Downs, J.J. Jauhal, S.K. Nandra, G.G. Prive, Sequence and structural analysis of BTB domain proteins, Genome Biol. 6 (10) (2005) R82.
[35] J. Adams, R. Kelso, L. Cooley, The kelch repeat superfamily of proteins: propellers of cell function, Trends Cell Biol. 10 (1) (2000) 17–24.
[36] P.J. Stogios, G.G. Prive, The BACK domain in BTB-kelch proteins, Trends Biochem. Sci. 29 (12) (2004) 634–637.
[37] A.T. Dinkova-Kostova, K.T. Liby, K.K. Stephenson, W.D. Holtzclaw, X. Gao, N. Suh, C. Williams, R. Risingsong, T. Honda, G.W. Gribble, M.B. Sporn, P. Talalay, Extremely potent triterpenoid inducers of the phase 2 response: correlations of protection against oxidant and inflammatory stress, Proc. Natl. Acad. Sci. U. S. A. 102 (12) (2005) 4584–4589.
[38] A. Cuadrado, M. Pajares, C. Benito, J. Jimenez-Villegas, M. Escoll, R. Fernandez-Gines, A.J. Garcia Yague, D. Lastra, G. Manda, A.I. Rojo, A.T. Dinkova-Kostova, Can activation of NRF2 Be a strategy against COVID-19? Trends Pharmacol. Sci. 41 (9) (2020) 598–610.
[39] R. Borella, L. Forti, L. Gibellini, A. De Gaetano, S. De Biasi, M. Nasi, A. Cossarizza, M. Pinti, Synthesis and anticancer activity of CDDO and CDDO-me, two derivatives of natural triterpenoids, Molecules 24 (22) (2019) 4097.
[40] H. Kanda, K. Yamawaki, Bardoxolone methyl: drug development for diabetic kidney disease, Clin. Exp. Nephrol. 24 (10) (2020) 857–864.
[41] J. Hu, Q. Xu, C. McTiernan, Y.C. Lai, D. Osei-Hwedieh, M. Gladwin, Novel targets of drug treatment for pulmonary hypertension, Am. J. Cardiovasc. Drugs 15 (4) (2015) 225–234.
[42] A. Mullard, FDA approves first Friedreich's ataxia drug, Nat. Rev. Drug Discov. (2023), https://doi.org/10.1038/d41573-023-00041-9.
[43] D.R. Lynch, M.P. Chin, M.B. Delatycki, S.H. Subramony, M. Corti, J.C. Hoyle, S. Boesch, W. Nachbauer, C. Mariotti, K.D. Mathews, P. Giunti, G. Wilmot, T. Zesiewicz, S. Perlman, A. Goldsberry, M. O'Grady, C.J. Meyer, Safety and

efficacy of omaveloxolone in Friedreich ataxia (MOXIe study), Ann. Neurol. 89 (2) (2021) 212–225.
[44] N.C. Payne, A.S. Kalyakina, K. Singh, M.A. Tye, R. Mazitschek, Bright and stable luminescent probes for target engagement profiling in live cells, Nat. Chem. Biol. 17 (11) (2021) 1168–1177.
[45] L. Baird, A.T. Dinkova-Kostova, Diffusion dynamics of the Keap1-Cullin3 interaction in single live cells, Biochem. Biophys. Res. Commun. 433 (1) (2013) 58–65.
[46] T. Iso, T. Suzuki, L. Baird, M. Yamamoto, Absolute amounts and status of the nrf2-keap1-cul3 complex within cells, Mol. Cell Biol. 36 (24) (2016) 3100–3112.
[47] K.I. Tong, Y. Katoh, H. Kusunoki, K. Itoh, T. Tanaka, M. Yamamoto, Keap1 recruits Neh2 through binding to ETGE and DLG motifs: characterization of the two-site molecular recognition model, Mol. Cell Biol. 26 (8) (2006) 2887–2900.
[48] P.D. Adams, P.V. Afonine, G. Bunkoczi, V.B. Chen, I.W. Davis, N. Echols, J. J. Headd, L.W. Hung, G.J. Kapral, R.W. Grosse-Kunstleve, A.J. McCoy, N. W. Moriarty, R. Oeffner, R.J. Read, D.C. Richardson, J.S. Richardson, T. C. Terwilliger, P.H. Zwart, PHENIX: a comprehensive Python-based system for macromolecular structure solution, Acta Crystallogr. D Biol. Crystallogr. 66 (Pt 2) (2010) 213–221.
[49] G. B.E Bricogne, M. Brandl, C. Flensburg, P. Keller, W. Paciorek, S.A. Roversi P, O. S. Smart, C. Vonrhein, T.O. Womack, BUSTER, Global Phasing Ltd., Cambridge, United Kingdom, 2011.
[50] P. Emsley, B. Lohkamp, W.G. Scott, K. Cowtan, Features and development of Coot, Acta Crystallogr. D Biol. Crystallogr. 66 (Pt 4) (2010) 486–501.
[51] V.B. Chen, W.B. Arendall 3rd, J.J. Headd, D.A. Keedy, R.M. Immormino, G. J. Kapral, L.W. Murray, J.S. Richardson, D.C. Richardson, MolProbity: all-atom structure validation for macromolecular crystallography, Acta Crystallogr. D Biol. Crystallogr. 66 (Pt 1) (2010) 12–21.
[52] Y. Cheng, W.H. Prusoff, Relationship between the inhibition constant (K1) and the concentration of inhibitor which causes 50 per cent inhibition (I50) of an enzymatic reaction, Biochem. Pharmacol. 22 (23) (1973) 3099–3108.
[53] E. Krissinel, K. Henrick, Inference of macromolecular assemblies from crystalline state, J. Mol. Biol. 372 (3) (2007) 774–797.
[54] N.C. Payne, S. Maksoud, B.A. Tannous, R. Mazitschek, A direct high-throughput protein quantification strategy facilitates discovery and characterization of a celastrol-derived BRD4 degrader, Cell Chem. Biol. 29 (8) (2022) 1333–1340 e5.
[55] N.C. Payne, R. Mazitschek, Resolving the deceptive isoform and complex selectivity of HDAC1/2 inhibitors, Cell Chem. Biol. 29 (7) (2022) 1140–1152 e5.
[56] N.C. Payne, R. Mazitschek, Tiny titans: nanobodies as powerful tools for TR-FRET assay development, Anal. Sens. 2 (6) (2022), e202200020.
[57] I. Jarmoskaite, I. AlSadhan, P.P. Vaidyanathan, D. Herschlag, How to measure and evaluate binding affinities, Elife 9 (2020), e57264.
[58] B.D. Wilson, H.T. Soh, Re-evaluating the conventional wisdom about binding assays, Trends Biochem. Sci. 45 (8) (2020) 639–649.
[59] T.G. Davies, W.E. Wixted, J.E. Coyle, C. Griffiths-Jones, K. Hearn, R. McMenamin, D. Norton, S.J. Rich, C. Richardson, G. Saxty, H.M. Willems, A.J. Woolford, J. E. Cottom, J.P. Kou, J.G. Yonchuk, H.G. Feldser, Y. Sanchez, J.P. Foley, B. J. Bolognese, G. Logan, P.L. Podolin, H. Yan, J.F. Callahan, T.D. Heightman, J. K. Kerns, Monoacidic inhibitors of the kelch-like ECH-associated protein 1: nuclear factor erythroid 2-related factor 2 (KEAP1:NRF2) protein-protein interaction with high cell potency identified by fragment-based discovery, J. Med. Chem. 59 (8) (2016) 3991–4006.
[60] P. Canning, A.N. Bullock, New strategies to inhibit KEAP1 and the Cul3-based E3 ubiquitin ligases, Biochem. Soc. Trans. 42 (1) (2014) 103–107.
[61] G. Rachakonda, Y. Xiong, K.R. Sekhar, S.L. Stamer, D.C. Liebler, M.L. Freeman, Covalent modification at Cys151 dissociates the electrophile sensor Keap1 from the ubiquitin ligase CUL3, Chem. Res. Toxicol. 21 (3) (2008) 705–710.
[62] A.L. Eggler, G. Liu, J.M. Pezzuto, R.B. van Breemen, A.D. Mesecar, Modifying specific cysteines of the electrophile-sensing human Keap1 protein is insufficient to disrupt binding to the Nrf2 domain Neh2, Proc. Natl. Acad. Sci. U. S. A. 102 (29) (2005) 10070–10075.
[63] A.L. Eggler, E. Small, M. Hannink, A.D. Mesecar, Cul3-mediated Nrf2 ubiquitination and antioxidant response element (ARE) activation are dependent on the partial molar volume at position 151 of Keap1, Biochem. J. 422 (1) (2009) 171–180.
[64] T. Ichikawa, J. Li, C.J. Meyer, J.S. Janicki, M. Hannink, T. Cui, Dihydro-CDDO-trifluoroethyl amide (dh404), a novel Nrf2 activator, suppresses oxidative stress in cardiomyocytes, PLoS One 4 (12) (2009), e8391.
[65] M.H. Wong, H.K. Bryan, I.M. Copple, R.E. Jenkins, P.H. Chiu, J. Bibby, N.G. Berry, N.R. Kitteringham, C.E. Goldring, P.M. O'Neill, B.K. Park, Design and synthesis of irreversible analogues of bardoxolone methyl for the identification of pharmacologically relevant targets and interaction sites, J. Med. Chem. 59 (6) (2016) 2396–2409.
[66] X. Meng, J.C. Waddington, A. Tailor, A. Lister, J. Hamlett, N. Berry, B.K. Park, M. B. Sporn, CDDO-Imidazolide targets multiple amino acid residues on the Nrf2 adaptor, Keap1, J. Med. Chem. 63 (17) (2020) 9965–9976.
[67] P. Wang, J. Song, D. Ye, CRL3s: the BTB-CUL3-RING E3 ubiquitin ligases, Adv. Exp. Med. Biol. 1217 (2020) 211–223.